Probing defect states in polycrystalline GaN grown on Si(111) by sub-bandgap laser-excited scanning tunneling spectroscopy

F.-M. Hsiao,[1,2] M. Schnedler,[2] V. Portz,[2] Y.-C. Huang,[3] B.-C. Huang,[4] M.-C. Shih,[1] C.-W. Chang,[1] L.-W. Tu,[1] H. Eisele,[5] R. E. Dunin-Borkowski,[2] Ph. Ebert,[2] and Y.-P. Chiu[1,4,6]
[1]*Department of Physics, National Sun Yat-sen University, Kaohsiung 80424, Taiwan*
[2]*Peter Grünberg Institut, Forschungszentrum Jülich GmbH, 52425 Jülich, Germany*
[3]*Department of Physics, National Cheng Kung University, Tainan 70101, Taiwan*
[4]*Institute of Physics, Academia Sinica, Taipei 11529, Taiwan*
[5]*Institut für Festkörperphysik, Technische Universität Berlin, Hardenbergstr. 36, 10623 Berlin, Germany*
[6]*Department of Physics, National Taiwan University, Taipei 10617, Taiwan*

(Received 31 August 2016; accepted 7 December 2016; published online 6 January 2017)

We demonstrate the potential of sub-bandgap laser-excited cross-sectional scanning tunneling microscopy and spectroscopy to investigate the presence of defect states in semiconductors. The characterization method is illustrated on GaN layers grown on Si(111) substrates without intentional buffer layers. According to high-resolution transmission electron microscopy and cathodoluminescence spectroscopy, the GaN layers consist of nanoscale wurtzite and zincblende crystallites with varying crystal orientations and hence contain high defect state densities. In order to discriminate between band-to-band excitation and defect state excitations, we use sub-bandgap laser excitation. We probe a clear increase in the tunnel current at positive sample voltages during sub-bandgap laser illumination for the GaN layer with high defect density, but no effect is found for high quality GaN epitaxial layers. This demonstrates the excitation of free charge carriers at defect states. Thus, sub-bandgap laser-excited scanning tunneling spectroscopy is a powerful complimentary characterization tool for defect states. *Published by AIP Publishing.* [http://dx.doi.org/10.1063/1.4972563]

INTRODUCTION

During recent years, nitride-based compound semiconductors turned out to be the first choice for energy efficient lighting applications, power electronics, and energy harvesting.[1] This wide range of applications has been made possible due to the achievement of *p*-type GaN[2,3] and the optimization of the epitaxy growth processes in order to reduce the density of dislocations.[4] The dislocation density depends strongly on the choice of the underlying substrate and buffer layers. Although highly efficient light-emitting diodes (LEDs) can be grown on free standing GaN, SiC, and Sapphire, the need for low cost devices increases the interest in nitride-based LEDs grown on cheap and large-sized Si substrates. As a drawback, the growth of GaN structures directly on Si substrates usually causes a high density of threading dislocations and cracks due to strong deviations of the lattice constants and the thermal expansion coefficients.[5–7] Hence, the defect characterization is a critical issue for optimization of nitride-based semiconductor devices.

In this paper, we present sub-bandgap laser excited cross-sectional scanning tunneling microscopy (STM) and spectroscopy (STS) as a new method for probing defects states, using GaN layers with a high defect state density and, for comparison, high quality GaN epitaxial layers. We demonstrate the detection of mid gap defect states with the help of laser-excited STS and correlate these with the microstructure probed by transmission electron microscopy (TEM) and the electronic properties characterized by cathodoluminescence (CL) measurements.

SAMPLES

For demonstrating the characterization potential of sub-bandgap laser-excited tunneling spectroscopy, we used relatively defect rich GaN layers (labeled defect-rich GaN/Si) grown directly on Si. The GaN layers with a thickness of 2.6 μm were grown on a *n*-type Si(111) [P: $5 \times 10^{18}\,\mathrm{cm}^{-3}$] substrate that was cleaned in acetone, isopropanol, and deionized water in an ultrasonic bath for 5 min. Moreover, the substrate was etched with hydrofluoric acid and heated *in-situ* to 800 °C for 15 min, in order to remove native oxides. Hence, clean 7×7 reconstructed Si(111) surfaces were obtained. The GaN layers were deposited by molecular beam epitaxy under nitrogen-rich conditions (N_2:Ga beam equivalent pressure ratio of 160) at 720 °C. The low temperature, nitrogen rich growth conditions were chosen to avoid the detrimental melt-back etching that is known to occur at higher temperatures and Ga-rich conditions.[7] The GaN layers can be expected to exhibit *n*-type conductivity due to unintentional doping.

For comparison, we also investigated a high-quality *n*-type GaN epitaxial layer grown by hydride vapor phase epitaxy (HVPE) labeled high quality GaN with a carrier concentration of $(1–3) \times 10^{18}\,\mathrm{cm}^{-3}$. The average dislocation density was below $2 \times 10^{7}\,\mathrm{cm}^{-2}$.[8] No grain boundaries were present and no deep level defect states occurred, with exception of areas directly in the center of v-shaped defects.[9] Outside of v-shaped defects the layers were of high quality and single crystalline.

Cross-sectional TEM

A bright-field high resolution transmission electron microscopy (HR-TEM) image of the interface region in the

defect-rich GaN/Si sample is shown in Fig. 1(a). The HR-TEM image is obtained along the $[11\bar{2}]$ zone axis (at the Si side). A 3–4 nm thick interface layer is detectable that separates the substrate (upper left part in Fig. 1(a)) from the defect-rich GaN layer (lower, darker part in Fig. 1(a)) and is marked by dashed lines. In view of the growth conditions (nitrogen-rich, low temperature growth), the presence of this interface layer indicates the formation of SiN_x during the initial growth of GaN, as has been frequently observed and reported in other works.[10–13]

The SiN_x interface layer exhibits polycrystalline as well as amorphous regions. Furthermore, the thickness of the SiN_x layer is fluctuating. These fluctuations may arise from meltback etching during the initial growth process.[7] As a result, polycrystalline GaN is formed during the further deposition process. This becomes evident by comparing the two areas highlighted by white rectangles in Fig. 1(a): Reciprocal space images of the first (labeled 1) and second (labeled 2) areas, derived by fast Fourier transforms (FFT), are displayed in Figs. 1(b) and 1(c), respectively. The reciprocal lattice belonging to the first area (Fig. 1(b)) corresponds to α-GaN (wurtzite structure), oriented along the $[10\bar{1}0]$ direction. In contrast, the reciprocal lattice of the second area (Fig. 1(c)) indicates the presence of β-GaN (zincblende structure), oriented along the $[\bar{1}11]$ direction. In general, the crystallites are elongated along the growth direction. Considering fluctuations in thickness of the TEM samples, the presence of overlapping crystallites, and surface contaminations, which all change the atomic scale intensity in the HR-TEM image in Fig. 1(a), the size of the crystallites can be estimated to be about 50 nm in the vicinity of the Si-GaN interface. The size increases further away from the Si-GaN interface.

Cathodoluminescence

The top-view CL measurements were performed using a JEOL JSM-7000F scanning electron microscope combined with a Gatan MonoCL (slit in/exit: 5 mm/5 mm, current: 20 nA, dwell time: 1 s, and grating: 1200 grooves/mm). The resulting CL spectra for the defect-rich GaN/Si sample, measured at different temperatures from 20 K up to room-temperature, are displayed in Fig. 2 in logarithmic scale. The main peak at ∼3.4 eV corresponds to the band-to-band transitions (excitons) and excitons bound to shallow defects.[14] As expected,[15] the peak shifts to smaller values with increasing temperature. A similar behaviour is found for the second order peak at ∼1.7 eV. The peak at ∼3.4 eV exhibits an unusually large width. In addition, a high CL intensity with flanks at ∼2.8 eV and at ∼2.6 eV as well as a notable intensity at ∼1.8 eV occurs. These CL intensities and the large peak width should not occur for high quality GaN layers. They point to the presence of many crystallites and different polytypes[16] and high defect densities, such as stacking faults, grain boundaries, and dislocations,[17] in agreement with the TEM images. All these defects will induce gap states. For example, density-functional tight-binding calculations yield defect states associated with grain boundaries over a wide energy range in the upper half of the band gap,[18] in agreement with the CL spectra.

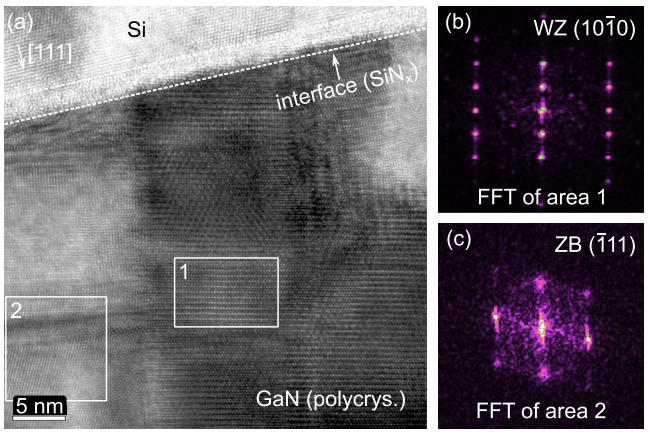

FIG. 1. (a) A high resolution transmission electron microscopy (HR-TEM) bright-field image of the interface region in the defect-rich GaN/Si sample (along the $[11\bar{2}]$ zone axis). A 3–4 nm thick interface layer that separates the substrate (upper left part) from the GaN layer (lower darker part) is visible and indicated by dashed lines. (b) Reciprocal space images of the area that is labeled with "1" in (a), derived by fast Fourier transform (FFT). The reciprocal lattice shows α-GaN (wurtzite structure), oriented along the $[10\bar{1}0]$ direction. (c) Reciprocal space image of the area that is labeled with "2" in (a), also obtained by FFT. The reciprocal lattice indicates the presence of β-GaN (zincblende structure), oriented along the $[\bar{1}11]$ direction.

SUB-BAND GAP LASER-EXCITED SCANNING TUNNELING MICROSCOPY AND SPECTROSCOPY

Experiment

For the laser-excited cross-sectional STM and STS investigations, the defect-rich GaN/Si samples were cleaved *in-situ* in a ultrahigh vacuum (UHV) at $\lesssim 1 \times 10^{-10}$ mbar to obtain contamination-free nominally $(11\bar{2})$-oriented Si surfaces for cross-sectional imaging of the defect-rich GaN/Si interface. The high-quality GaN layer was cleaved directly on its $(10\bar{1}0)$ *m*-plane. The cross-sectional STM and STS measurements of the defect-rich GaN/Si sample and the high quality HVPE grown GaN layer were performed at ∼100 K and at room temperature, respectively, with an Omicron variable temperature STM (VT-STM) using tungsten tips and without interruption of the vacuum. For the laser-excited measurements, the defect-rich GaN/Si sample was

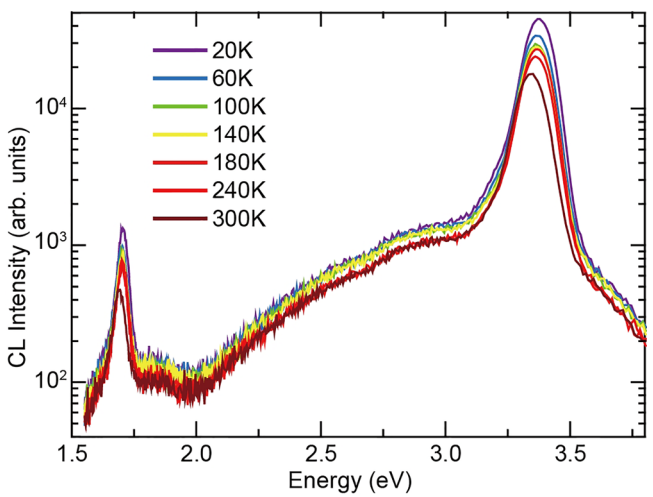

FIG. 2. Top-view cathodoluminescence spectra measured on the growth plane of the defect-rich GaN/Si sample at different temperatures.

illuminated 60° off-normal to the surface by a 405 nm diode-laser module with a power of 3.9 mW (see Fig. 3(a)). Focusing of the beam was achieved by a build-in lens. According to the spot size on the sample surface, we estimated a laser irradiance of $\sim 2.5 \times 10^5\,\mathrm{W\,m^{-2}}$. For the high-quality GaN sample, we used the same geometric setup, but a 1 mW laser with build-in lens. The laser irradiance at the tip position was $\sim 1.5 \times 10^5\,\mathrm{W\,m^{-2}}$.

The laser setup was used for two different tunneling spectroscopy acquisition modes: First, XSTM images or $I(V)$ spectra can be obtained under constant laser illumination. Second, an optical chopper (not shown in Fig. 3(a)) was employed to periodically interrupt the laser beam with a frequency of $\geq$400 Hz to obtain simultaneously tunnel currents with and without light excitation during the acquisition of a single $I(V)$ spectrum at constant tip-sample separation. For the mechanically driven optical chopper, we derived envelope functions to separate the tunnel currents under illumination from those under dark conditions.[19] For the electronically controlled chopper, we turned on and off the laser, acquiring directly spectra with and without light excitation separately.[20] In order to minimize thermal expansion effects,[21] we installed the sample surface closest possible to the thermally compensated plane of the VT-STM. In addition, we used a low laser irradiance and a chopper with a period length significantly shorter than the time constant of thermal heating. This ensures that the tip-sample separation is not affected by the irradiation.

The photon energy of the diode laser was chosen to be below the fundamental band gap of GaN. Hence, direct band-to-band transitions can be excluded within the GaN layer. Thus, excitation of electron-hole pairs requires electronic states within the fundamental band gap and hence any excitation by the sub bandgap laser illumination can be related to defect states.

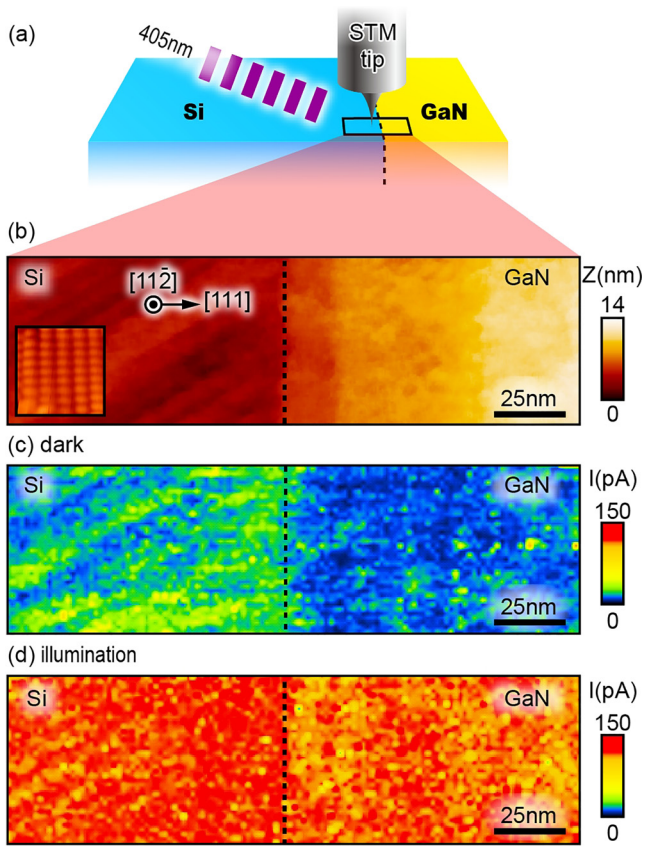

FIG. 3. (a) Experimental setup of our light-excited cross-sectional STM/STS setup. Measurements can be obtained under constant illumination or by employing an optical chopper that periodically interrupts the laser beam with a frequency of 400 Hz. (b) Constant-current cross-sectional STM image (acquired at −3 V and 150 pA) of the Si/GaN interface region without illumination. The position of the interface is indicated by the black dashed line. Inset: Constant-current STM image (acquired at −0.9 V and 800 pA) of the 2×1 reconstructed Si(111) surface. Si has the tendency to form terraces exhibiting these surfaces, when cleaved on (11$\bar{2}$) planes. (c) and (d) Current-imaging tunneling spectroscopy (CITS) maps across the Si/GaN interface (c) without and (d) with constant illumination measured at a tip-sample separation defined by a set voltage of −3 V and a set tunnel current of 150 pA. We chose a negative set-voltage since the tunnel current remains unchanged under illumination at negative voltages and hence the feedback controller does not alter the tip-sample separation due to illumination based effects. The images are evaluated for a voltage of +3.0 V.

Results

Figure 3(b) illustrates a cross-sectional constant-current STM image showing the filled states of the interface region within the defect-rich GaN/Si sample without illumination acquired at a (sample) voltage of −3 V and a tunnel current of 150 pA. The position of the GaN/Si interface is indicated by the black dashed line. The interface position shows up by a pronounced topography change and by differences in the electronic properties on both materials. First, we turn to the topography changes:

On the Si side, a high density of 1 to 5 ML high steps is present. These steps arise from a preferential cleavage along {111} planes when attempting to cleave Si on (11$\bar{2}$) planes. This is corroborated by atomically resolved STM images obtained on similarly cleaved Si wafers, where a clear 2×1 reconstruction of Si(111) oriented terraces is visible [inset in Fig. 3(b)].[22] In contrast to the Si cleavage surface, fewer steps are present on the GaN surface, which are oriented parallel to the interface and have heights of up to 1.6 nm. The interface region itself shows up as a depression.

The cross-section view imaged by STM (within the Si substrate) is identically oriented as the HR-TEM images in Fig. 1(a). The particular sample region imaged by STM exhibits a rather smooth GaN area. This suggests that in this region a GaN *m*-plane cleavage surface was obtained, since the *m* plane is the only smooth cleavage surface of wurtzite structure GaN.[23–27] This local configuration is similar to that in the area 1 of the HR-TEM image in Fig. 1(a).

In addition, current-imaging tunneling spectroscopy (CITS) was performed across the defect-rich Si/GaN interface with and without constant illumination (i.e., without optical chopper). We chose a negative set-voltage (−3 V) since the tunnel current remains unchanged under illumination at negative voltages and hence the feedback controller does not alter the tip-sample separation due to illumination effects. Figures 3(c) and 3(d) show the CITS images evaluated at a voltage of +3.0 V without and with illumination, respectively. In the dark as well as under illumination, the tunnel current in the GaN layer is slightly smaller than that on the Si substrate. The change of the electronic properties

occurs at the same position, where the topography changes. This location is identified as interface position and marked as dashed lines.

Figure 4(a) shows as an example a tunneling spectrum acquired on GaN 30 nm away from the interface in the dark (black symbols) and under illumination (red symbols) using an optical chopper for the defect-rich GaN layer on Si. For comparison, Fig. 4(b) shows a set of spectra for the high quality GaN layer, measured as in Ref. 20 with a similar irradiance of $\sim 1.5 \times 10^5\,\mathrm{W\,m^{-2}}$. No effect due to illumination occurs on the high quality GaN layer, whereas a pronounced illumination effect is observed on the defect-rich GaN layer on Si.

Discussion

Without illumination, the $I(V)$ spectra exhibit similar features to previous spectra measured on non-polar GaN$(10\bar{1}0)$ surfaces only modulated by different tip-sample separations and different tip shapes and geometries, which affect the intensity and apparent onset of the accumulation current.[28,29] For both samples, the tunneling spectra exhibit an apparent band gap (voltage range without tunnel current) smaller than the fundamental band gap. This indicates that no extrinsic pinning is present. Hence, only a voltage-dependent pinning at small positive voltages due to the intrinsic empty surface state is present as found previously for GaN cleavage surfaces.[28,29] These effects are, however, not relevant for the present discussion.

Instead, the central result of the tunneling spectra in Fig. 4 is that under sub-bandgap laser illumination the tunnel current shows a significant increase at positive voltages only for the defect-rich GaN layers grown on Si but not for high-quality GaN layers. Thus, for defect-rich GaN layers the free charge carrier concentration must increase when illuminated with photons, whose energy is smaller than the fundamental band gap of GaN.

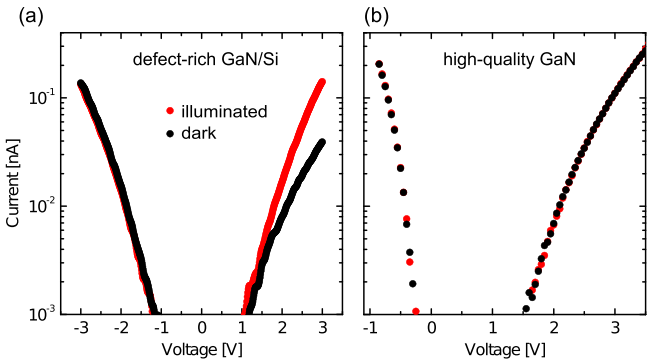

FIG. 4. Tunneling spectra acquired in the dark (black symbols) and under laser illumination (red symbols) (a) 30 nm away from the GaN/Si interface on the defect-rich GaN layer and (b) on the high quality GaN layers. (a) and (b) were acquired using mechanical and electronic optical choppers, respectively. The irradiances of the 405 nm laser were (a) $\sim 2.5 \times 10^5\,\mathrm{W\,m^{-2}}$ and (b) $\sim 1.5 \times 10^5\,\mathrm{W\,m^{-2}}$. The tip-sample separations were defined by a voltage and current of (a) −3 V and 150 pA and (b) +3 V and 100 pA, respectively. The tip-sample separation is identical for the spectra in the dark and under illumination. Only for the defect rich GaN layer, sub-bandgap laser illumination increases the tunnel current, due to excitation of electrons from defect states.

Since the samples differ in their substrate (Si versus GaN), we first have to address a possible influence of the Si substrate. The central question here is, if the additional free charge carriers detectable in the sub bandgap illuminated GaN layer originate from band-to-band excitation in the Si substrate. In principle, electrons/holes photo excited in the Si substrate by direct band-to-band transitions could diffuse into the GaN layer. This would increase the free electron/hole concentration, lower the tip-induced band bending, and hence increase the tunnel current as previously discussed.[20,30,31] In order to elucidate this, we turn to a three-dimensional electrostatic simulation of the potential distribution and carrier concentrations of an ideal GaN/Si junction.[20,30] The simulation based on the finite difference method assumes perfect crystallinity as well as the absence of defect states and of an insulating SiN_x layer. We further assumed a dopant concentration of $5 \times 10^{18}\,\mathrm{cm^{-3}}$ for the substrate, as specified by the manufacturer, and a small, unintentional doping ($\sim 10^{17}\,\mathrm{cm^{-3}}$) for the GaN layer. On the GaN surface, we include an empty S_{Ga} surface state within the band gap as found previously.[28,29,32,33] The surface state was modelled as a Gaussian density of states distribution with a FWHM of 0.3 eV and a peak energy 0.59 eV below the conduction band edge. We assume that the occupation of the surface state is in thermal equilibrium with the Fermi-level. At the Si surface, we include the presence of the π bonded chain states in the fundamental band gap,[34] which are responsible for the observed pinning.[35] For the calculation, we used a volume of $(250 \times 250 \times 250)\,\mathrm{nm^3}$ with a non-uniform mesh and a minimal point separation of 0.25 nm. The boundary and interface conditions are the same as those described in Refs. 20, 30, and 36.

The results of the simulation are exemplified for a voltage of +2.0 V in Fig. 5: The band alignment and the electron concentration across the interface at the cleavage surface (dashed lines) and 100 nm away from the surface in the bulk (solid lines) are illustrated in Figs. 5(a) and 5(b), respectively. In these graphs, black (red) lines correspond to the results without (with) illumination. Figures 5(c) and 5(d) show the spatial distribution of the electrostatic potential and the electron concentration of the system under illumination perpendicular to the surface, respectively.

The simulated band diagram in Fig. 5(a) demonstrates that neither holes nor electrons can cross the Si-GaN junction in relevant concentrations. The insignificant electron/hole diffusion from Si to GaN can be explained as follows: GaN and Si exhibit similar electron affinities of ∼4.1 eV but strongly different band gaps. Hence, in the bulk, the conduction bands of Si and GaN are almost aligned, while a strong discontinuity is present for the valence bands. This enable in principle (excited) electrons to freely cross the Si/GaN interface, while (excited) holes have to remain in the Si substrate. However, when electrons start to diffuse into the GaN layer, an electrical field is created at the interface due to the lack of positive charge carriers on the GaN side. The electric field counteracts the diffusion process, similar to the field that is created in the depletion zone of a *p-n* junction. Hence, the

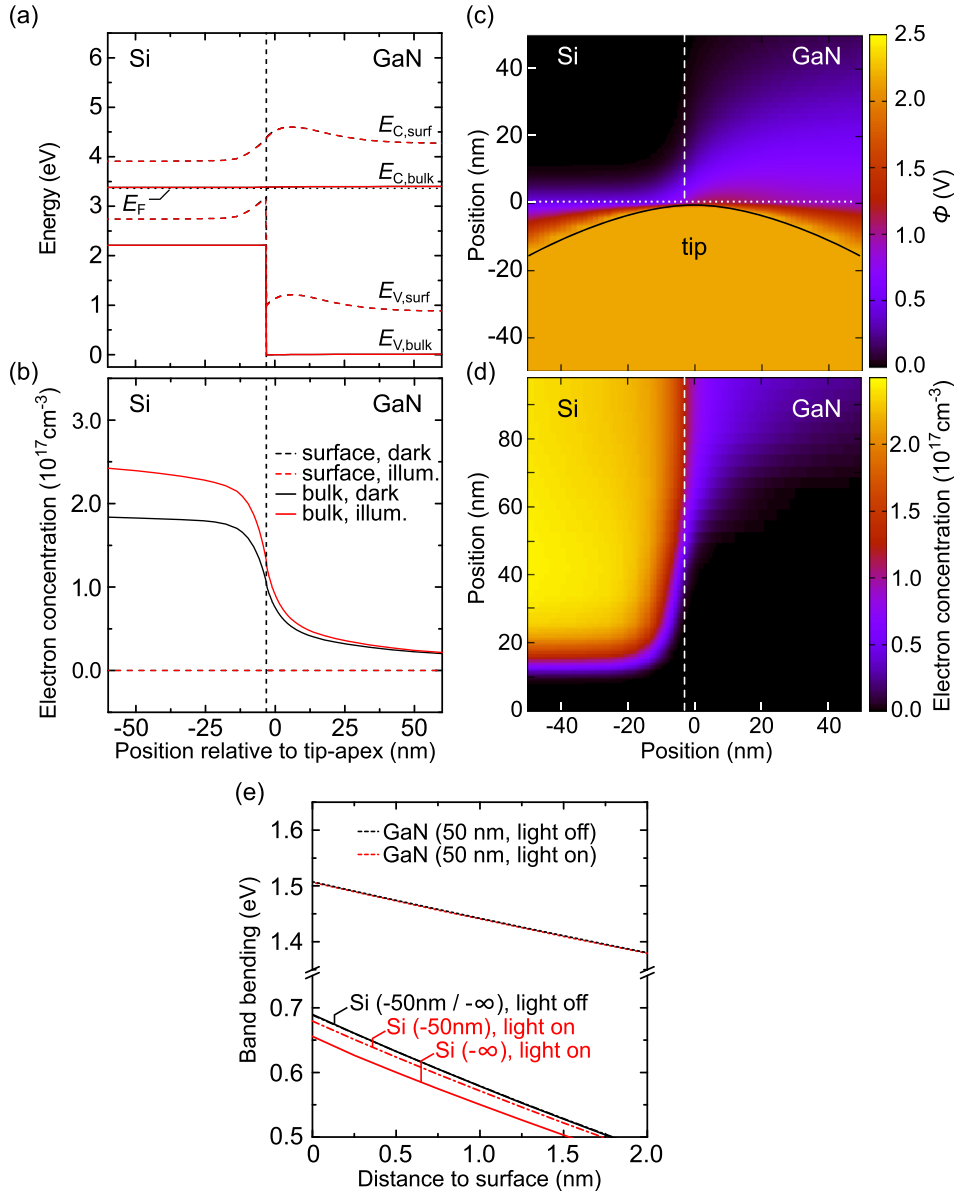

FIG. 5. Simulation of an ideal tip-vacuum-cross-sectional GaN/Si system (voltage: +2.0 V), assuming no SiN_x layer. The tip is positioned 3 nm away from the GaN/Si interface on the GaN side (position 0 nm). The GaN/Si interface is indicated by the vertical dashed lines. The cleavage surface is marked in (c) by the horizontal white dotted line. (a) Band alignment and (b) electron concentration across the interface at the cleavage surface (dashed lines) and 100 nm below the surface in the bulk (solid lines). Black lines correspond to the results without illumination. Band alignments and electron concentrations for a laser irradiance of $E_e = 2.5 \times 10^5$ W m^{-2} are shown as dark red lines in (a) and (b). (c) Spatial distribution of the electrostatic potential under illumination (Φ relative to GaN) of the system along a plane perpendicular to the surface through the tip apex. (d) Lateral distribution of the electron concentration under illumination on the same plane. (e) Tip-induced band bending vs. depth near the surface for the tip positioned above pure Si (solid), Si 50 nm away from the interface (dashed-dotted), and GaN 50 nm away from the interface (dotted) for a voltage of +2 V. The band bending in the dark and under illumination is shown as black and red curves, respectively. The difference of the band bending directly at the surface between the dark and illuminated state gives the surface photovoltage. No surface photovoltage is found for GaN, indicating the absence of laser-excited carriers in GaN.

electron concentration in the GaN layer cannot be increased significantly.

The quantitative values in Fig. 5(b) show that the electron concentration in the GaN layer ~100 nm below the surface (solid lines) increases for the experimentally used laser irradiance of 2.5×10^5 W m^{-2} by only 5×10^{15} cm^{-3}, leaving the total electron concentration below 5×10^{16} cm^{-3}. At the GaN cleavage surface (assumed to be *m*-plane in the simulation), the partially occupied Ga-derived dangling bond state and the positive voltage lead to an upward band bending as shown by the dashed lines in Fig. 5(a). This causes a strong lowering of the electron concentration near the GaN surface (cf. dashed lines in Fig. 5(b)) and additionally hinders excited electrons to cross the Si/GaN interface in this region. Hence, independent of the illumination, the electron and hole concentrations in the vicinity of the GaN surface are negligible.

Therefore, we do not expect any change of the tunnel current under illumination for a high-quality defect-free GaN layer when $I(V)$ spectra are obtained some nanometers away from the interface. This is corroborated by the surface photovoltage (i.e., the change of the tip-induced band bending

under illumination), which is only present in Si, but not in GaN as illustrated in the calculated band bending in Fig. 5(e) for +2 V. The band bending is reduced for laser-excited Si. In contrast, the band bending and hence band edges are unchanged for GaN and therefore no change in the tunnel current occurs during illumination. This theoretical result is further strengthened by the presence of the SiN_x layer at the interface, which was not included in the simulation and should further impede the transport of excited electrons through the interface.

Based on the conclusions that no electron can be directly excited from the valence into the conduction band and that insignificant electron densities diffuse from the Si substrate into the GaN layer, another excitation mechanism is required. Instead, excited electrons or holes can be created directly in the GaN layer by exciting electrons from filled defect states in the fundamental band gap into the conduction band or by exciting electrons from the valence band into ionized defect states, respectively. This trap-assisted carrier generation can take place already with sub-bandgap excitation.[37,38] Defect states or traps are indeed present in the defect-rich GaN layers grown on Si. The CL spectra in Fig. 2 show a wide distribution of defect states in the fundamental band gap. The defect-related excitation is furthermore corroborated by the absence of any illumination effect for the high-quality GaN layers, where no high defect concentrations are present. Hence, the sub-bandgap laser excitation enables tunneling spectroscopy to probe defects states in the band gap.

CONCLUSION

In summary, sub-bandgap laser-excited cross-sectional scanning tunneling microscopy and spectroscopy is applied to investigate the presence of defect states in GaN layers. The characterization method is illustrated using defect-rich GaN layers grown on Si(111) substrates without intentional buffer layers and high-quality GaN layers with low defect concentrations. High-resolution transmission electron microscopy and cathodoluminescence spectroscopy of the defect-rich GaN layers grown on Si(111) substrates reveal the presence of nanoscale wurtzite and zincblende crystallites with varying crystal orientations as well as high densities of grain boundaries and dislocations and high defect state densities. A clear increase in the tunnel current at positive voltages is observed during sub-bandgap laser illumination for the GaN layer with high defect density, but no effect is found for high quality GaN epitaxial layers. This demonstrates the excitation of charge carriers at defect states, increasing the free charge carrier concentration and lowering the tip-induced band bending to which the scanning tunneling spectroscopy is sensitive. This work demonstrates that sub-bandgap laser-excited scanning tunneling spectroscopy is a powerful complimentary characterization tool for defect states. By extending it to a wave length dependent measurement, it will become possible to combine the high spatial resolution of the STM with the capability to identify defects with optical spectroscopy accessing gap states.

ACKNOWLEDGMENTS

The authors thank the Ministry of Science and Technology (MOST), Taiwan (Project Nos. 104-2112-M-002-025-MY3, 103-2112-M-002-028-MY3, and 104-2911-I-003-514), the Helmholtz-Gemeinschaft Deutscher Forschungszentren (Impuls- und Vernetzungsfond, Grant No. HIRG-0014), and the Deutsche Forschungsgemeinschaft (Collaborative Research Center Sfb 787, TP A4) for financial support.

[1]H. Morkoç, *Nitride Semiconductor Devices: Fundamentals and Applications* (John Wiley & Sons, 2013).
[2]S. Nakamura, T. Mukai, M. Senoh, and N. Iwasa, Jpn. J. Appl. Phys., Part 1 **31**, L139 (1992).
[3]S. Nakamura, S. Pearton, and G. Fasol, *The Blue Laser Diode: The Complete Story* (Springer, 2000), p. 34, ISBN 9783540665052.
[4]G. Li, W. Wang, W. Yang, Y. Lin, H. Wang, Z. Lin, and S. Zhou, Rep. Prog. Phys. **79**, 056501 (2016).
[5]A. Dadgar, J. Bläsing, A. Diez, A. Alam, M. Heuken, and A. Krost, Jpn. J. Appl. Phys., Part 2 **39**, L1183 (2000).
[6]A. Dadgar, M. Poschenrieder, J. Blasing, K. Fehse, A. Diez, and A. Krost, Appl. Phys. Lett. **80**, 3670 (2002).
[7]B. Zhang and Y. Liu, Chin. Sci. Bull. **59**, 1251 (2014).
[8]P. H. Weidlich, M. Schnedler, H. Eisele, R. Dunin-Borkowski, and Ph. Ebert, Appl. Phys. Lett. **103**, 142105 (2013).
[9]P. H. Weidlich, M. Schnedler, H. Eisele, U. Strauß, R. E. Dunin-Borkowski, and Ph. Ebert, Appl. Phys. Lett. **103**, 062101 (2013).
[10]B. Yang, A. Trampert, O. Brandt, B. Jenichen, and K. H. Ploog, J. Appl. Phys. **83**, 3800 (1998).
[11]T. A. Rawdanowicz and J. Narayan, Appl. Phys. Lett. **85**, 133 (2004).
[12]G. Radtke, M. Couillard, G. A. Botton, D. Zhu, and C. J. Humphreys, Appl. Phys. Lett. **100**, 011910 (2012).
[13]D. Zhu, D. J. Wallis, and C. J. Humphreys, Rep. Prog. Phys. **76**, 106501 (2013).
[14]M. A. Reshchikov and H. Morkoç, J. Appl. Phys. **97**, 061301 (2005).
[15]V. Bougrov, in *Gallium Nitride (GaN)*, edited by M. E. Levinshtein, S. L. Rumyantsev, and A. Zubrilov (John Wiley and Sons, 2001), pp. 1–30.
[16]M. Suzuki, T. Uenoyama, and A. Yanase, Phys. Rev. B **52**, 8132 (1995).
[17]F. A. Ponce, D. P. Bour, W. Gotz, and P. J. Wright, Appl. Phys. Lett. **68**, 57 (1996).
[18]A. Béré, P. Ruterana, G. Nouet, A. T. Blumenau, S. Sanna, T. Frauenheim, J. Chen, and J. Koulidiati, Phys. Rev. B **71**, 125211 (2005).
[19]O. Takeuchi, S. Yoshida, and H. Shigekawa, Appl. Phys. Lett. **84**, 3645 (2004).
[20]M. Schnedler, V. Portz, P. H. Weidlich, R. E. Dunin-Borkowski, and Ph. Ebert, Phys. Rev. B **91**, 235305 (2015).
[21]S. Grafström, J. Appl. Phys. **91**, 1717 (2002).
[22]R. M. Feenstra, W. A. Thompson, and A. P. Fein, Phys. Rev. Lett. **56**, 608 (1986).
[23]L. Ivanova, S. Borisova, H. Eisele, M. Dähne, A. Laubsch, and Ph. Ebert, Appl. Phys. Lett. **93**, 192110 (2008).
[24]Ph. Ebert, L. Ivanova, S. Borisova, H. Eisele, A. Laubsch, and M. Dähne, Appl. Phys. Lett. **94**, 062104 (2009).
[25]M. Bertelli, P. Löptien, M. Wenderoth, A. Rizzi, R. G. Ulbrich, M. C. Righi, A. Ferretti, L. Martin-Samos, C. M. Bertoni, and A. Catellani, Phys. Rev. B **80**, 115324 (2009).
[26]D. Krüger, S. Kuhr, T. Schmidt, D. Hommel, and J. Falta, Phys. Status Solidi RRL **3**, 91 (2009), ISSN 1862-6270.
[27]H. Eisele and Ph. Ebert, Phys. Status Solidi RRL **6**, 359 (2012), ISSN 1862-6270.
[28]L. Lymperakis, P. H. Weidlich, H. Eisele, M. Schnedler, J.-P. Nys, B. Grandidier, D. Stievenard, R. E. Dunin-Borkowski, J. Neugebauer, and Ph. Ebert, Appl. Phys. Lett. **103**, 152101 (2013).
[29]M. Schnedler, V. Portz, H. Eisele, R. E. Dunin-Borkowski, and Ph. Ebert, Phys. Rev. B **91**, 205309 (2015).
[30]M. Schnedler, R. E. Dunin-Borkowski, and Ph. Ebert, Phys. Rev. B **93**, 195444 (2016).
[31]P. Kloth, K. Kaiser, and M. Wenderoth, Nat. Commun. **7**, 10108 (2016).

[32]M. Himmerlich, A. Eisenhardt, S. Shokhovets, S. Krischok, J. Räthel, E. Speiser, M. D. Neumann, A. Navarro-Quezada, and N. Esser, Appl. Phys. Lett. **104**, 171602 (2014).
[33]M. Landmann, E. Rauls, W. G. Schmidt, M. D. Neumann, E. Speiser, and N. Esser, Phys. Rev. B **91**, 035302 (2015).
[34]J. A. Stroscio, R. M. Feenstra, and A. P. Fein, Phys. Rev. Lett. **57**, 2579 (1986).
[35]F. J. Himpsel, G. Hollinger, and R. A. Pollak, Phys. Rev. B **28**, 7014 (1983).
[36]S. Selberherr, *Analysis and Simulation of Semiconductor Devices* (Springer, Vienna, New York, 1984).
[37]R. N. Hall, Phys. Rev. **87**, 387 (1952).
[38]W. Shockley and W. T. Read, Phys. Rev. **87**, 835 (1952).